Discrete Time Modeling of Spherical Harmonic Expansion by Using Band-Limited Step Functions

Nara Hahn[1] and Sascha Spors[2]

[1] *Division of Applied Acoustics, Chalmers University of Technology, Gothenburg, Sweden*

[2] *Institute of Communications Engineering, University of Rostock, Rostock, Germany*

Email: `nara.hahn@chalmers.se`, `sascha.spors@uni-rostock.de`

Introduction

In spherical harmonics expansion of a homogeneous sound field, the radial components are described by spherical Bessel functions in the frequency domain [1]. The time-domain counterparts are Legendre polynomials windowed by a rectangular pulse [2, 3, 4, 5]. Since the discontinuity occurring at the edge of the rectangular window exhibits an infinite bandwidth, a discrete-time signal obtained by trivial sampling exhibits aliasing artifacts. Therefore, the resulting spectral distortions are likely to affect the performance of applications that are based on time-domain representations [6, 7].

In this paper, an analytical anti-aliasing filtering is applied to the time-domain radial functions in order to reduce aliasing. The presented method is adopted from [8, 9, 10, 11] which was primarily proposed for digital synthesis of analog synthesizer sounds such as square waves and sawtooth waves. The discontinuities of the radial functions are replaced by smooth transient responses thus limiting the bandwidth. The band-limited radial functions thus can be sampled with considerably reduced aliasing artifacts. While this paper only considers the radial functions for plane waves, the presented approach can be used for spherical waves as well [2].

Nomenclature Vectors (position and direction) are represented in spherical coordinates $\boldsymbol{x} = (r, \theta, \phi)$, with $r \geq 0$ denoting the radius, $\theta \in [0, \pi]$ the colatitude, and $\phi \in [0, 2\pi)$ the azimuth. Angular frequency is denoted by $\omega = 2\pi f$ where f is the temporal frequency in Hz. The imaginary unit is denoted by i ($i^2 = -1$). The speed of sound is assumed to be $c = 343$ m/s, and the sampling frequency is set to $f_\mathrm{s} = 44.1$ kHz.

Continuous Time Representations

Consider the sound field of a plane wave propagating in the direction $\boldsymbol{n}_\mathrm{pw} = (1, \theta_\mathrm{pw}, \phi_\mathrm{pw})$. The frequency-domain representation of the spherical harmonics expansion reads [1, Eq. (6.175)]

$$e^{-i\frac{\omega}{c} r \cos\Theta} = \sum_{n=0}^{\infty} (2n+1) i^{-n} j_n(\tfrac{\omega}{c} r) P_n(\cos\Theta), \qquad (1)$$

where the sound field is expanded at the origin and evaluated at $\boldsymbol{x} = (r, \theta, \phi)$. For each order n, the angular (directional) dependency is described by the Legendre polynomial $P_n(\cdot)$, and the radial dependency by the spherical Bessel function of the first kind $j_n(\cdot)$. The latter are called the radial (basis) functions. The angle between $\boldsymbol{x}$ and $\boldsymbol{n}_\mathrm{pw}$ is denoted by Θ, i.e. $\cos\Theta = \cos\theta\cos\theta_\mathrm{pw} + \sin\theta\sin\theta_\mathrm{pw}\cos(\phi - \phi_\mathrm{pw})$.

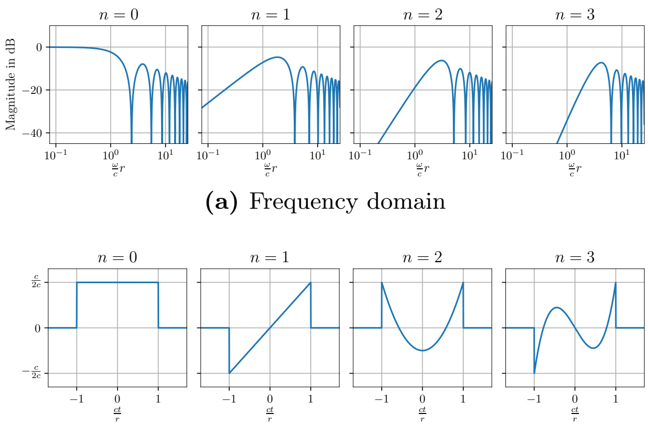

(a) Frequency domain

(b) Time domain

Figure 1: Radial functions in (a) frequency-domain (magnitude) $i^{-n} j_n(\frac{\omega}{c} r)$ and (b) time-domain $\frac{c}{2r}\tilde{P}_n(\frac{c}{r}t)$. Frequency axes are scaled by $\frac{r}{c}$ and the time axes by $\frac{c}{r}$.

The time-domain representation of (1) reads [5]

$$\delta\big(t - \tfrac{r}{c}\cos\Theta\big) = \frac{c}{2r} \sum_{n=0}^{\infty} (2n+1) \tilde{P}_n(\tfrac{c}{r}t) P_n(\cos\Theta), \qquad (2)$$

where the time-domain radial functions $\tilde{P}_n(\frac{c}{r}t)$ coincide with the Legendre polynomials $P_n(\frac{c}{r}t)$ for $|t| < \frac{r}{c}$ and vanishes elsewhere, i.e.

$$\tilde{P}_n(\tfrac{c}{r}t) := \begin{cases} P_n(\frac{c}{r}t), & |t| < \frac{r}{c} \\ 0, & |t| > \frac{r}{c}. \end{cases} \qquad (3)$$

This follows from the Fourier transform relationship $\mathcal{F}\{\frac{c}{2r}\tilde{P}_n(\frac{c}{r}t)\} = i^{-n} j_n(\frac{\omega}{c} r)$ [12, Eq. (10.59.1)]. The term i^{-n} is included in the frequency-domain radial function so that the time-domain radial functions are real-valued.

In Fig. 1(a), the magnitude of the frequency-domain radial functions are depicted. For $\frac{\omega}{c} r \gg n$, the peak values decay with -6 dB/octave regardless of the order, which corresponds to the large argument approximations $j_n(z) \approx \frac{1}{z}\sin(z - \frac{n\pi}{2})$ [12, Eq. (10.52.3)]. Note that the temporal frequency spectrum is not band limited. The time-domain radial functions are shown in Fig. 1(b). While the functions are continuous and smooth within the interval $|t| < \frac{r}{c}$, jump discontinuities occur at $|t| = \frac{r}{c}$

which results in the infinite bandwidth of the radial functions.

Sampling and Aliasing

While the continuous-time representations (2) might be suitable for theoretical studies, practical applications [6, 7] typically require a discrete-time model with acceptable accuracy. A time discretization can be carried out most straightforwardly by a uniform sampling of the continuous-time representation, which leads to periodic repetitions of the spectrum in the frequency domain [13, Sec. 4.2]. Due to the infinite bandwidth of the radial functions, cf. Fig. 1(a), the repeated spectra inevitably overlap with the baseband spectrum resulting in aliasing artifacts. This section investigates the influence of aliasing on the temporal and spectral characteristics of discrete-time radial functions that are obtained by uniform sampling.

As depicted in Fig. 1(b), the time-domain radial functions are Legendre polynomials windowed by a rectangular pulse,

$$\frac{c}{2r}\tilde{P}_n(\tfrac{c}{r}t) = \frac{c}{2r}\Big[u(t+\tfrac{r}{c}) - u(t-\tfrac{r}{c})\Big]P_n(\tfrac{c}{r}t) \tag{4}$$

where $u(t)$ denotes the unit step function,

$$u(t) := \begin{cases} 0, & t < 0 \\ 1, & t > 0. \end{cases} \tag{5}$$

Assume that (4) is sampled at discrete time instances,

$$t_k = k \cdot T_\mathrm{s}, \quad k \in \mathbb{Z}, \tag{6}$$

with $T_\mathrm{s} = 1/f_\mathrm{s}$ denoting the sampling interval. The discontinuous points $t = \pm\frac{r}{c}$ are generally fractional multiples of T_s, thus quantized in the discrete time domain. This effect is demonstrated in Fig. 2(a) for a single unit step function $u(t-\tau)$ with varying time shift τ. As t is scaled by f_s, the sample index k can be read from the axis. It can be seen that the discrete-time signals (indicated by ●) are identical for the considered fractional sample shifts $\frac{\tau}{T_\mathrm{s}} = 0.25, 0.50, 0.75$. Although not shown here, this is also the case for $k < \frac{\tau}{T_\mathrm{s}} < k+1$ where $k \in \mathbb{Z}$.[1] This implies that the width of the sampled radial functions generally deviate from $\frac{2r}{c}$.

In Fig. 3, the spectra of the discrete-time radial functions (—) are compared with the exact frequency-domain radial functions $i^{-n} j_n(\frac{\omega}{c}r)$ (■) and the deviations (—) are depicted. Due to the non-causality of the representation (2), an integer sample delay $e^{-i\omega L f_\mathrm{s}}$ ($L\, f_\mathrm{s} > \frac{r}{c}$, $L \in \mathbb{Z}_+$) is applied to the complex spectra.

Figure 3(a) shows the 0th-order radial function for different radii. The increase of spectral distortions is apparent for smaller r, where more spectral components lie in $|\omega| > \pi f_\mathrm{s}$ ($|f| > 22.05$ kHz) thus contributing to aliasing.

[1] One might argue that the sampled values should be determined based on the nearest integer of $\frac{\tau}{T_\mathrm{s}}$. This constitutes a 0th-order interpolation which is subsumed under the approach introduced in the next section.

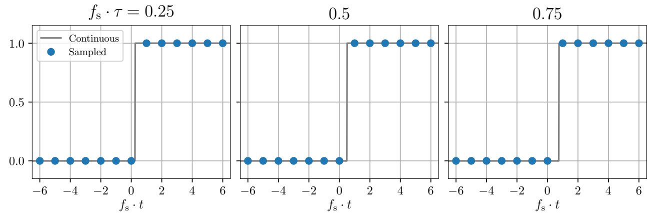

(a) Unit step function

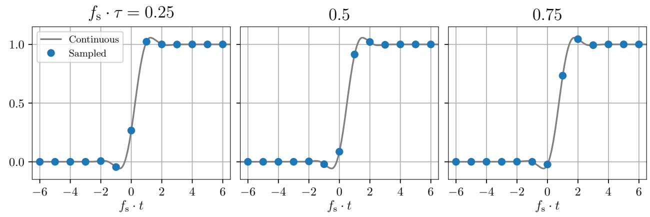

(b) Lagrange BLEP function

Figure 2: Sampling of (a) unit step function and (b) BLEP function derived from a 5th-order Lagrange polynomial. Different fractional sample shifts $\frac{\tau}{T_\mathrm{s}} = 0.25, 0.5, 0.75$ are considered. The discrete-time samples ($t_k = k \cdot T_\mathrm{s}$) are indicated by ●.

While uniform sampling might be acceptable for large r, care must be taken if the sound field is evaluated close to the origin (small r). The slight boost around $\omega = \pi f_\mathrm{s}$ is attributed to the nearest spectral repetitions occurring at $\pm 2\pi f_\mathrm{s}$. Since $P_0(\cdot) = 1$, cf. Fig. 1(b), the DC response is determined by the width of the 0th-order radial function. The distortions at $\omega \to 0$ thus result from the aforementioned deviations of the discontinuities. The latter also lead to spectral zeros that differ from those of the exact spectrum. Notice that the peaks of the distortion coincide with the zeros of the spectrum.

The radial functions of different orders $n = 1, 2, 3$ are shown in Fig. 3(b) for $r = 0.1$. At high frequencies, the peak of the spectral distortions exhibits similar characteristics (including the case of $n = 0$ shown in Fig. 3(a)). Due to the zeros of the radial functions at $\omega = 0$, the lower spectrum is dominated by aliasing artifacts.

A trivial countermeasure against aliasing distortions is to increase the sampling rate so that the repeated spectra are sufficiently apart from each other. The spectral overlap is thereby reduced which further benefits from the attenuation of the spherical Bessel functions for large arguments [12, Eq. (10.52.3)]. This improvement, however, comes at the expense of computations which scales with the oversampling factor.

Band Limited Step Functions

Aliasing can be reduced more effectively by applying an analytical low-pass filtering to continuous-time representations [14]. Once a band-limited radial function is obtained in closed form, it can be sampled with reduced spectral distortions. In this paper, the approach introduced in [10, 11] is employed and adapted to the time-domain radial functions.

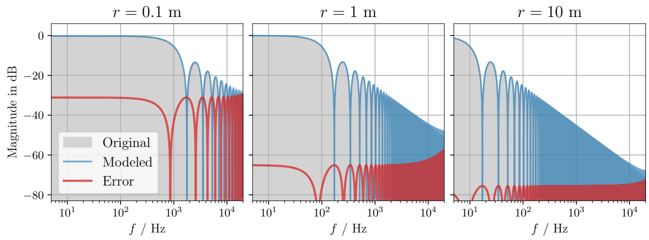

(a) $n = 0$ and $r = 0.1, 1, 10$ m

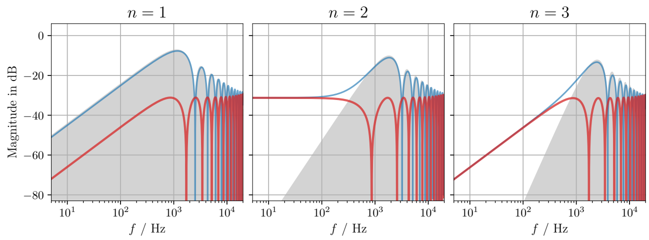

(b) $n = 1, 2, 3$ and $r = 0.1$ m

Figure 3: Frequency spectra of discrete-time radial functions without bandwidth limitation.

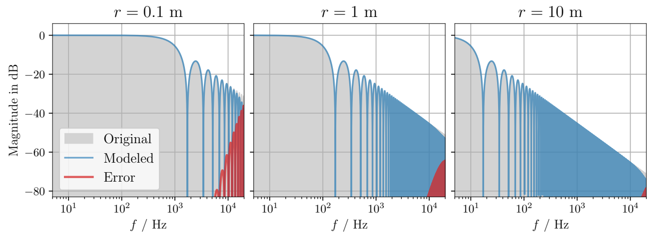

(a) $n = 0$ and $r = 0.1, 1, 10$ m

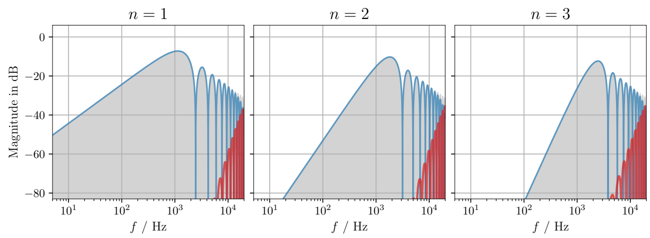

(b) $n = 1, 2, 3$ and $r = 0.1$ m

Figure 4: Frequency spectra of band-limited discrete-time radial functions. BLEP functions are derived from 5th-order Lagrange polynomials.

Note from (4) that the 0th-order radial function can be represented as a superposition of two unit step functions. A single unit step function can be represented as the running integral of the Dirac delta function [15, p. 93],

$$u(t-\tau) = \int_{-\infty}^{t} \delta(t'-\tau)\mathrm{d}t' \qquad (7)$$

for an arbitrary time shift τ. Convolving both sides with the impulse response of a low-pass filter $h(t)$ yields

$$u_h(t-\tau) = \int_{-\infty}^{t} h(t'-\tau)\mathrm{d}t', \qquad (8)$$

which is called the band-limited step (BLEP) function defined as [9, 11, 14]

$$u_h(t) \coloneqq u(t) *_t h(t) \qquad (9)$$

with $*_t$ denoting convolution.

Equation (8) states that a BLEP function $u_h(t)$ can be obtained by integrating an appropriately chosen $h(t)$.[2] The impulse response $h(t)$ should be piecewise continuous and bounded so that the resulting BLEP function (its integration) does not exhibit discontinuities. Otherwise, the discretization would lead to aliasing artifacts as observed in the previous section. To assure $u_h(\infty) \to 1$, the impulse response must satisfy $\int_{-\infty}^{\infty} h(t')\mathrm{d}t' = 1$.

As introduced in [14], BLEP functions can be derived from interpolation polynomials. The impulse response $h(t)$ is expressed by piecewise polynomials within a finite interval. Integrating the closed-form $h(t)$ yields a BLEP function whose transient response is also of finite length. In this paper, BLEP functions based on Lagrange interpolation are used [10, 11]. For the sake of simplicity, only odd-order N interpolation is considered. Interested readers are referred to the original articles [10, 11] for detailed discussion.

[2]BLEP functions based on digital filters are also available [14], where the integration is performed numerically. The scope of the present paper is on continuous-time BLEP functions.

In this approach, the band-limited impulse response $h(t)$ constitutes an interpolation of a discrete-time unit impulse $\delta[k]$. For the interval $t \in [t_k, t_{k+1}]$, an Nth-order interpolation exploits $N+1$ samples (nodes),

$$\delta[k - \tfrac{N-1}{2}], \dots, \delta[k], \delta[k+1], \dots, \delta[k + \tfrac{N+1}{2}] \qquad (10)$$

where $\frac{N+1}{2}$ samples lie on each side of t. The interpolated signal $h_k(t)$ for this interval is a weighted sum of those samples [16, p. 41],

$$\begin{aligned} h_k(t) &= \sum_{l \in \mathcal{S}_k} \delta[l] \prod_{m \in \mathcal{S}_k \setminus \{l\}} \frac{t - \tilde{t}_m}{\tilde{t}_l - \tilde{t}_m} \\ &= \prod_{m \in \mathcal{S}_k \setminus \{0\}} \frac{t - \tilde{t}_m}{\tilde{t}_0 - \tilde{t}_m} \\ &= \prod_{m \in \mathcal{S}_k \setminus \{0\}} \frac{m - \frac{t}{T_s}}{m} \end{aligned} \qquad (11)$$

where $\mathcal{S}_k \coloneqq \{k - \frac{N-1}{2}, \dots, k + \frac{N+1}{2}\}$. In the second equality, $\delta[k \neq 0] = 0$ is exploited and (6) is used in the third equality. Since $h_k(t)$ vanishes for $0 \notin \mathcal{S}_k$, the impulse response needs to be derived only for a finite number of intervals,

$$h(t) = \begin{cases} h_k(t), & k \in [-\frac{N+1}{2}, \frac{N+1}{2}] \\ 0, & \text{otherwise}, \end{cases} \qquad (12)$$

where each $h_k(t)$ is a polynomial of order N. The impulse response thus has a finite extent, $-\frac{N+1}{2} < \frac{t}{T_s} < \frac{N+1}{2}$, implying that the bandwidth is not ideally limited. A thorough discussion on the spectral properties of Lagrange interpolators are found in [17].

Expanding and integrating the factored form (11) reveals the BLEP function which is a piecewise polynomial of order $N+1$. The integral constant in each interval has to be determined in such a way that the BLEP function is continuous [11]. Since the polynomial coefficients only depend on the interpolation order N, they can be precomputed. Arbitrary time shift τ can be applied to the BLEP function by substituting t with $t-\tau$, while keeping in mind that the individual intervals have to be shifted accordingly, $[t_k+\tau, t_{k+1}+\tau]$.

In Fig. 2(b), a BLEP function based on 5th-order Lagrange polynomial (BLEP function is of 6th order) is depicted. The jump discontinuities are modeled by smooth transient responses with finite lengths. Notice that the fractional sample shifts are appropriately modeled. Due to the non-ideal band limitation, however, spectral distortions are to be expected.

Band Limited Radial Functions

A low-pass filtered 0th-order radial function can be represented by using BLEP functions,

$$\frac{c}{2r}\tilde{P}_0(\tfrac{c}{r}t) *_t h(t) = \frac{c}{2r}\Big[u_h(t+\tfrac{r}{c}) - u_h(t-\tfrac{r}{c})\Big]. \quad (13)$$

The discrete-time radial function is obtained by sampling (13). The radial functions for higher orders $n \geq 1$ are then computed by using the recurrence relation of the Legendre polynomials [12, Eq. (14.10.3)],

$$\begin{aligned}(n+2)&P_{n+2}(\tfrac{c}{r}t) = \\ &(2n+3)(\tfrac{c}{r}t)P_{n+1}(\tfrac{c}{r}t) - (n+1)P_n(\tfrac{c}{r}t). \quad (14)\end{aligned}$$

The improvements achieved by Lagrange BLEP functions are demonstrated in Fig. 4. The 0th-order radial functions are shown in Fig. 4(a) for different radii. In comparison with Fig. 3(a), spectral distortions are reduced in the entire frequency band. Even for the smallest radius $r = 0.1$, the spectral deviation remains below -60 dB up to 10 kHz. Magnitude roll-offs occur at high frequencies mainly due to the non-ideal low-pass filtering. The spectral notches (zeros) are in close agreement with the exact spectrum, implying that the width of the signal is modeled accurately. For higher-order radial functions, shown in Fig. 4(b), the improved accuracy at low frequencies are noticeable. The peak envelope of aliasing spectrum barely changes for the considered orders $n \leq 3$.

Conclusion

In this paper, an approach for discrete-time modeling of spherical harmonics expansion is introduced. In order to reduce the spectral distortions caused by aliasing, an analytical low-pass filtering is applied to the continuous-time radial functions, where the impulse response of the low-pass filter is derived based on Lagrange polynomial interpolation. By sampling the band limited representations, discrete-time radial functions are obtained with substantially improved spectral accuracy. Numerical examples show that 5th-order interpolation is able to achieve a fairly good accuracy even for the most critical case (small radius).

References

[1] E. Williams, *Fourier Acoustics: Sound Radiation and Nearfield Acoustical Holography.* Academic Press, 1999.

[2] O. M. Buyukdura and S. S. Koc, "Two alternative expressions for the spherical wave expansion of the time domain scalar free-space Green's function and an application: Scattering by a soft sphere," *J. Acoust. Soc. Am. (JASA)*, vol. 101, no. 1, pp. 87–91, 1997.

[3] S. A. Azizoglu, S. S. Koc, and O. M. Buyukdura, "Spherical wave expansion of the time-domain free-space dyadic green's function," *IEEE Trans. Antennas Propag.*, vol. 52, no. 3, pp. 677–683, 2004.

[4] J. Li and B. Shanker, "Time-dependent Debye-Mie series solutions for electromagnetic scattering," *IEEE Trans. Antennas Propag.*, vol. 63, no. 8, pp. 3644–3653, 2015.

[5] N. Hahn and S. Spors, "Time-domain representations of a plane wave with spatial band-limitation in the spherical harmonics domain," in *Proc. 45th German Annu. Conf. Acoust. (DAGA)*, Rostock, Germany, Mar. 2019.

[6] N. Hahn, F. Winter, and S. Spors, "2.5D local wave field synthesis of a virtual plane wave using a time domain representation of spherical harmonics expansion," in *Proc. 23rd Int. Congr. Acoust. (ICA)*, Aachen, Germany, Sep. 2019.

[7] H. Sun, T. D. Abhayapala, and P. N. Samarasinghe, "Time domain spherical harmonic analysis for adaptive noise cancellation over a spatial region," in *IEEE Int. Conf. Acoust. Speech Signal Process. (ICASSP).* IEEE, 2019, pp. 516–520.

[8] T. Stilson and J. O. Smith, "Alias-free digital synthesis of classic analog waveforms." in *Int. Comput. Music Conf.*, Hong Kong, 1996.

[9] E. Brandt, "Hard sync without aliasing," in *Proc. Int. Comput. Music Conf.*, Havana, Cuba, 2001, pp. 365–368.

[10] J. Nam, V. Valimaki, J. S. Abel, and J. O. Smith, "Efficient antialiasing oscillator algorithms using low-order fractional delay filters," *IEEE Trans. Audio Speech Lang. Process.*, vol. 18, no. 4, pp. 773–785, 2009.

[11] V. Välimäki, J. Pekonen, and J. Nam, "Perceptually informed synthesis of bandlimited classical waveforms using integrated polynomial interpolation," *J. Acoust. Soc. Am. (JASA)*, vol. 131, no. 1, pp. 974–986, 2012.

[12] F. W. J. Olver, D. W. Lozier, R. F. Boisvert, and C. W. Clark, *NIST Handbook of Mathematical Functions Handback.* Cambridge University Press, 2010.

[13] A. V. Oppenheim, R. W. Schafer, and J. R. Buck, "Discrete-time signal processing," *Prentice Hall*, 1999.

[14] V. Valimaki and A. Huovilainen, "Antialiasing oscillators in subtractive synthesis," *IEEE Signal Process. Mag.*, vol. 24, no. 2, pp. 116–125, 2007.

[15] G. B. Arfken and H. J. Weber, *Mathematical Methods for Physicists.* Academic Press, 2005.

[16] T. I. Laakso, V. Valimaki, M. Karjalainen, and U. K. Laine, "Splitting the unit delay," *IEEE Signal Process. Mag.*, vol. 13, no. 1, pp. 30–60, 1996.

[17] A. Franck and K. Brandenburg, "A closed-form description for the continuous frequency response of Lagrange interpolators," *IEEE Sig. Process. Lett.*, vol. 16, no. 7, pp. 612–615, 2009.